Korean J. Chem. Eng., **28**(8), 1688-1692 (2011)
DOI: 10.1007/s11814-011-0031-7

Effect of Fe^{3+} doping on the performance of TiO_2 mechanocoated alumina bead photocatalysts

Cyril Jose Escopete Bajamundi*, Maria Lourdes Pascual Dalida*, Kitirote Wantala, Pongtanawat Khemthong***, and Nurak Grisdanurak****,†**

*Department of Chemical Engineering, College of Engineering, University of the Philippines, Diliman 1101, Philippines
**Department of Chemical Engineering, Faculty of Engineering, Khon Kaen University, Khon Kaen 40002, Thailand
***National Nanotechnology Center, NSTDA, Pathumthani 12120, Thailand
****NCE for Environmental and Hazardous Waste Management, Faculty of Engineering, Thammasat University, Pathumthani 12120, Thailand
(*Received 5 June 2010 • accepted 5 February 2011*)

Abstract−Ferric ion was introduced to the commercial photocatalyst P25 (Degussa) by ultrasonic wet impregnation technique. The concentration of the dopant was varied from 0.0 to 3.0% Fe/Ti ratio. The doped TiO_2 was then loaded to alumina balls using mechanical coating technique and followed by calcination in air at 400, 450, 500 and 550 °C. The fabricated photocatalyst was characterized by X-ray diffraction, N_2 adsorption-desorption isotherms, scanning electron microscopy, UV-Vis diffuse reflectance spectroscopy, X-ray adsorption near edge structure and photoluminescence spectroscopy. The photocatalytic activity was tested by following the degradation of methylene blue (MB). It was found that the Fe^{3+} doped TiO_2/Al_2O_3 has a combination of anatase and rutile phase and free of iron oxide phases. The optimum calcination temperature is 400 °C with 0.1% Fe^{3+} concentration. The catalyst addresses the entrainment in photocatalytic reactors, eliminating the need for a post filtration process.

Key words: TiO_2, Fe^{3+} Dopant, Mechanical Coating Technique, Al_2O_3 Beads

INTRODUCTION

Photocatalysis is being considered as an effective process under the class of advanced oxidation process. In recent years, many studies have been reported involving the use of TiO_2-based photocatalyst due to the physical and chemical stability, low cost, non-toxicity and unique electronic and optical properties of titania [1-4].

However to fully apply TiO_2-based photocatalyst for large scale applications, several issues should first be addressed. TiO_2 exhibits low quantum efficiency due to the short life span of the generated electron and hole (250 ns) [5]. Increasing the life of charge carriers would greatly contribute to enhance the efficiency of the catalyst. One possible method to accomplish this is to introduce trace amounts of metal or nonmetal ion dopants. For the case of metal ion, the increase in photocatalytic activity rates can be attributed to the ability of these ions to scavenge electrons on the photocatalyst surface. This leads to the decrease in electron-hole recombination. Choi et al. performed a systematic study of 21 metal ion dopants in quantum-sized TiO_2 colloids and reported that Fe^{3+} dopant gave the highest increase in activity [6]. The increased performance is attributed to the ability of Fe^{3+} ion to act as shallow charge trap in the TiO_2 lattice [7] and to increase the surface oxygen deficient sites where peroxide and superoxide species can form.

Another issue that must be addressed is reactor scale-up. Catalyst entrainment in slurry photoreactors is a major problem; thus hallow-fiber membrane ultra filtration is required to capture the photocatalyst. This is undesirable, in terms of process economics, due to the increase in the capital investment of such a scheme. Immobilizing the TiO_2 to a support addresses this concern. Yoshida et al. first reported the use of mechanical coating technique (MCT) followed by calcination to immobilize Ti in alumina bead. Via this process, Ti reacts with the O species in alumina to produce TiO_2 bound on the support. However, calcination temperature was reported to be one of main parameters. The calcination at high temperature (higher than 500 °C) may generate higher rutile phase, resulting in lower degradation [8].

In this work, TiO_2 was first doped with Fe^{3+} via wetness impregnation technique followed by subsequent coating to alumina via MCT and calcination. The synthesized catalyst was investigated in terms of its structure and surface properties and photocatalytic activity by following the degradation of methylene blue (MB).

EXPERIMENTAL

1. Fabrication of Alumina Bead Supported Fe-doped TiO_2

Iron (III) nitrate nonahydrate, $Fe(NO_3)_3 \cdot 9H_2O$ (99.0-100% assay from Merck) was used as the Fe^{3+} source. A given amount of the iron source was dissolved in acetone and stirred until complete dissolution. The ratio of Fe^{3+} ion and TiO_2 was adjusted according to 0.0, 0.1, 1.0 and 3.0 atomic percentages. Each sample was assigned as $Fe_x/TiO_2/Al_2O_3$, where x represents the concentration of the dopant.

The solution was then mixed to 5 g of Degussa P25 using Elma ultrasonic mixer at 100% intensity for 30 min. Thereafter, the solution was left overnight to dry in an oven at 100 °C. The dried sample was carefully ground to homogenize the size of the powder. The fine powder and the alumina balls (particle size 0.5-1.2 mm, WHA-104 from Pingxiang Huihua Packing Co., Ltd., China) were intro-

†To whom correspondence should be addressed.
E-mail: gnurak@engr.tu.ac.th

duced to a steel pot for milling; the milling time was 15 h at 300 rpm. To study the effect of calcination temperature the catalyst balls were calcined in an electric muffler furnace (JSR Model JSMF-30T) at 400, 450, 500 and 550 °C for 20 h.

2. Analysis of Catalyst Properties

The supported catalyst was analyzed for its crystal structure and phase using powder X-ray diffraction (XRD), Bruker D8, equipped with a Cu Kα radiation source (wavelength 1.5406 Å). All of the powder samples were run at a scanning range of 20-60° with an increment of 0.02° and a step time of 2.0 s. To determine the light absorption of the catalysts, UV-visible absorbance spectra using Hitachi UV3501 with a wavelength range of 200-800 nm and $BaSO_4$ was used as the standard. The morphology of the catalyst balls was also examined by scanning electron microscope, JEOL JSM-6400, and the surface area was evaluated by using N_2 adsorption-desorption isotherm, Quantachrome, Autosorb I. Photoluminescence spectra were recorded with Perkin Elmer, LS 55, at room temperature under the excitation light at 315 nm.

The X-ray adsorption near edge structure (XANES) spectra were recorded using a double Ge (2 2 0) crystal monochromator for selection of photon energy. The data were obtained at room temperature in fluorescent mode with a 13-element Ge detector. The photon energy was calibrated by an Fe foil at 7111.2 eV and scanned from −30 eV below the edge to +80 eV above the edge. The XANES spectra were analyzed by using the Athena program.

3. Evaluation of Photocatalytic Activity

Photocatalytic activity was evaluated by measuring the decomposition of the probe pollutant-methylene blue (MB). The 0.3 g catalyst balls were spread uniformly at the bottom of a cylindrical glass cell (∅=2.25 cm and h=2.5 cm). 7 ml of 20 ppm MB (initial pH= 7) solution was then added to the cell. The cells were then irradiated with UV light using an 18-W Toshiba fluorescent lamp (wavelength of peak emission ~370 nm). The distance between the lamp and the reactor cell was 20 cm. Samples were collected at 2, 4, 6, 8, 12, 16, 20, and 24 h. The concentration of MB was measured using UV-Vis (Jasco-V630). The degradation efficiency (DE%) was calculated according to the following equation:

$$\text{Degradation Efficiency DE}(\%) = \frac{A_o - A}{A_o} \times 100\%$$

where A_o represents the absorbance of MB solution before irradiation and A represents the absorbance of the MB solution after being irradiated.

RESULTS AND DISCUSSION

1. Crystal Structure and Phase Using XRD

Phase composition of the catalyst and the crystalline size were evaluated from XRD patterns. The molar ratio of the anatase and rutile phases was determined from XRD peak intensity ration outlined by Spurr and Myers. The anatase and rutile phase intensities (I_A, I_R) of each sample were considered at 2θ of 25.6 and 27.5, respectively [9].

Fig. 1(a) shows the XRD patterns of $Fe_{0.1}/TiO_2/Al_2O_3$ calcined at different temperatures. It reveals a large decrease in the anatase phase as the calcination temperature is increased because the rutile phase is more stable at higher temperatures. Based on the results, calcination at 400 °C gave the highest percentage of anatase. This means that calcination beyond this temperature may prove detrimental to the photocatalytic ability of the catalyst (as discussed in section 3.6) and uneconomical because more energy is invested but the product is a less active catalyst. At this point, it should be noted that the anatase phase, being the more active and useful phase in terms photocatalysis, should be maintained as high as possible to attain optimum photocatalytic performance.

In addition, the x-ray diffractogram of the alumina is presented in Fig. 1(a). A peak registered at 2θ=68.20° indicating the presence of a α-β phase activated alumina [10].

Fig. 1(b) shows the XRD patterns of $Fe_x/TiO_2/Al_2O_3$ (x=0.0-3.0) calcined at 400 °C. Although it is believed that the rutile phase is not as effective as anatase for photocatalysis because the electron-hole recombination rate is much higher in rutile than in anatase, the optimum mixture of these two phases can have synergistic effect, thus increasing the photoactivity of the catalyst. As seen from Table 1, the content of rutile significantly changes for samples with Fe^{3+} content of 0.1 to 1.0%. This suggested that the phase transition was very pronounced and the change in %rutile could be attributed to partial loss of crystallinity with simultaneous partial rutile formation. In addition, no variation of the peaks corresponding to (211) crystallographic plane (54°) was detected as the concentration of the dopant was increased. Li et al. suggested that this was a rough indication that the dopant ions either occupied the interstitial sites

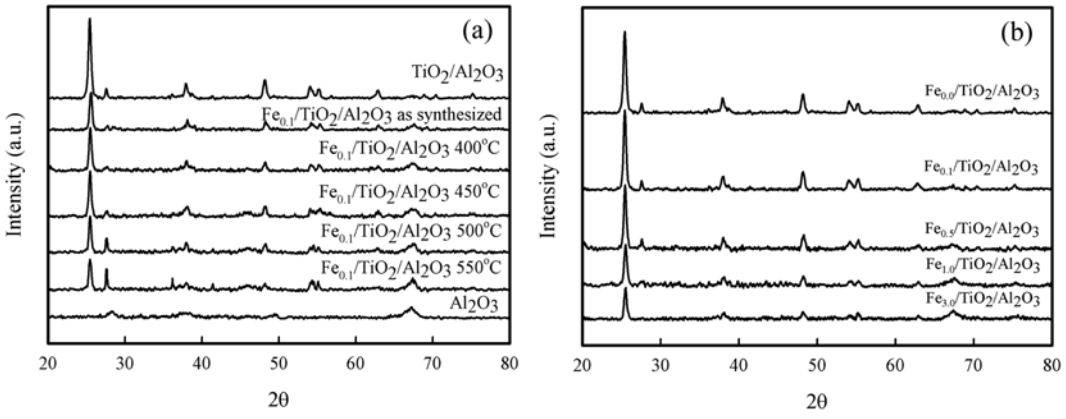

Fig. 1. XRD patterns of (a) $Fe_{0.1}/TiO_2/Al_2O_3$ calcined at different temperatures (b) $Fe_x/TiO_2/Al_2O_3$ beads calcined at 400 °C.

Table 1. Effects of Fe-dopant concentration on the physical properties of $Fe_x/TiO_2/Al_2O_3$ beads

Sample: $Fe_x/TiO_2/Al_2O_3$	Phase content (A/R)	Crystalline size* (nm)	Surface srea (m^2/g)
x=0.0	80/20	20.91	288
x=0.1	95/5	24.71	228
x=1.0	96/4	23.21	231
x=3.0	86/14	21.18	244

*Calculated from Scherrer equation

within the lattice or they substituted Ti^{4+} but without important distortion of the lattice. This is highly plausible since the radii of Ti^{4+} (0.68 Å) and Fe^{3+} (0.64 Å) ions are very similar [11]. In addition this claim can further be supported by the fact that no iron oxide or Fe_xTiO_y phases are found in the XRD patterns which should register a high peak at 2θ~35.0° (JCPDS Card #19-629).

2. Morphologies of the Photocatalyst

Selected microphotographs of Al_2O_3, $Fe_x/TiO_2/Al_2O_3$ (x=0.0, 0.1) are shown in Fig. 2. The morphology of the as-received Al_2O_3 presented rougher than other prepared catalysts. It exhibits numerous small valleys and peaks, giving it higher surface area (~340 m^2/g), compared to other prepared catalysts (~220-290 m^2/g).

On the other hand, the morphologies of the $Fe_x/TiO_2/Al_2O_3$ samples were somewhat smooth; this could be attributed to the surface smoothing effect induced by the mechanochemical coating technique. In addition, the surface became smoother as the amount of Fe^{3+} doping increased; this could be seen from the micrographs taken at higher magnification (2,000 : 1). The surface area of the catalyst with Fe^{3+} did not significantly change; doping may prevent particle agglomeration, forming well-defined nanocrystalline powders thus preventing too much change in the surface area.

3. UV-vis Diffuse Reflectance Spectra

Considering the catalyst with fixed Fe concentration (0.1%) calcined at different temperatures, Fig. 3(a) reveals a small increase in light absorption in visible region compared to $Fe_{0.0}/TiO_2/Al_2O_3$. It also reveals that the calcination temperature does not drastically alter the reflectance spectra of the samples. This is in agreement with the observation of Zhou et al. [12] that the red shift is a strong function of the doping concentration.

The effect of the doping concentration on the light absorption characteristics has also been studied and is shown in Fig. 3(b). It was found that as Fe^{3+}-doping concentration increases, the samples exhibit an increase in absorption of light in the visible range. Red shift in the band gap transition energy was also observed: 2.95 eV,

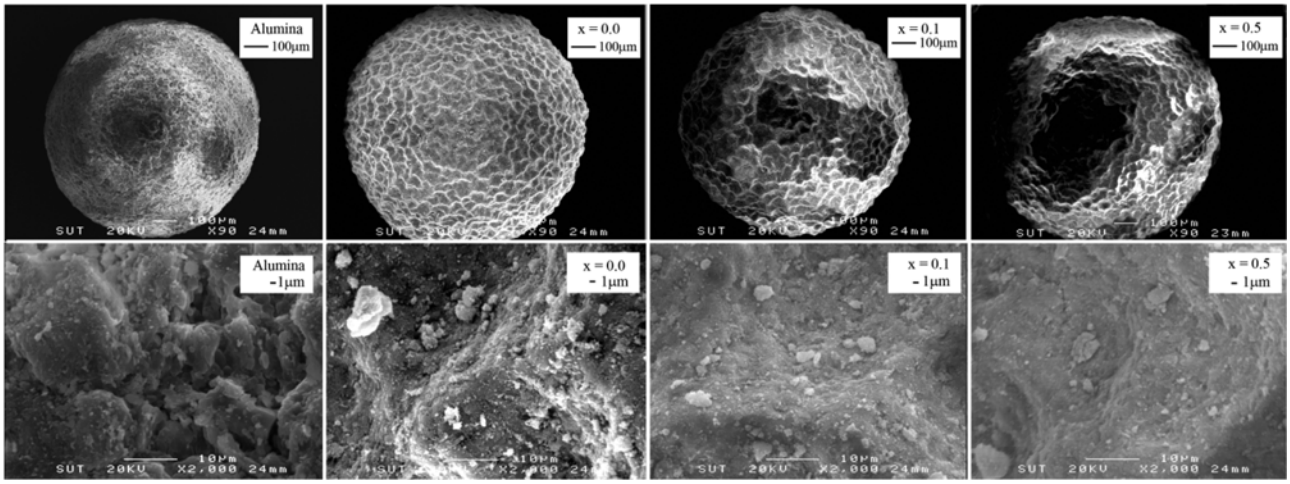

Fig. 2. SEM images of alumina and $Fe_x/TiO_2/Al_2O_3$ beads.

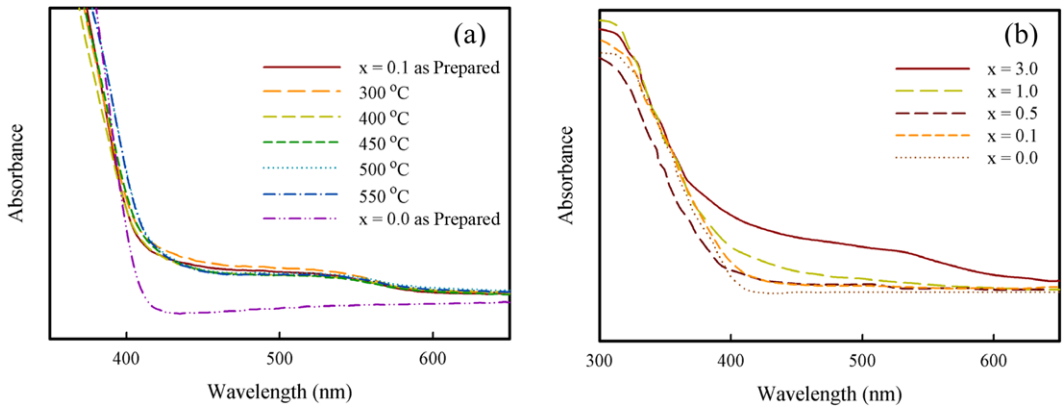

Fig. 3. UV-DR spectra of (a) $Fe_{0.1}/TiO_2/Al_2O_3$ beads calcined at different temperatures (b) Fe_x-TiO_2/Al_2O_3 beads calcined at 400 °C.

2.86 eV, 2.80 eV and 2.76 eV for x=0.0, 0.1, 0.5, 1.0 and 3.0, respectively. This spectral red shift originated from the excitation of 3d electrons from ferric ions into the conduction band of the semiconductor [13], which allowed TiO_2 to absorb light in the visible region. However this does not mean that high red shift is always favorable, because electrons trapped in the dopants have lower energy than anatase conducting band edge electrons, which results in a lower reducing capacity. This is true because photocatalytic process systems can be considered similar to an electrochemical cell; the decrease in band gap results in a decrease in the free energy change of the redox process occurring in the system [11].

4. Photoluminescence (PL) Spectra

The PL process is helpful in understanding the efficiency of charge carrier trapping, migration and transfer [14]. Photoluminescence is produced when the charge carriers are captured by impurities or recombine with another carrier. In this work, photoluminescence was measured via photoluminescence spectroscopy, where the light emission is measured as a function of the wavelength of the emitted light using a constant energy excitation source (excitation wavelength=315 nm using He-Cd laser).

The PL spectra of $Fe_{0.0}/TiO_2/Al_2O_3$ and $Fe_{0.1}/TiO_2/Al_2O_3$ in Fig. 4 exhibit wide and strong signal emission spectra at the UV and visible range with obvious peaks at about 390, 426 and 487 nm. For each of the wavelengths mentioned the intensity of the PL spectra for $Fe_{0.1}/TiO_2/Al_2O_3$ is lower compared to that of $Fe_{0.0}/TiO_2/Al_2O_3$. This could be ascribed to the restricted recombination of the charge carrier due of the incorporation or substitution on Fe^{3+} in the lattice of TiO_2. Fe^{3+} ion can easily accept the electrons from the conduction band of TiO_2 because of the small difference of the Fermi level between the semiconductor and the dopant. In addition, non-dissociative adsorption of molecular oxygen can occur due to the production of under coordinated sites due to Fe^{3+}-Ti^{4+} substitution [15]. The adsorbed O_2 can scavenge electrons producing superoxide species, which is demonstrated by the peak at 487 nm. These factors could enhance quantum efficiency, which translates to higher photoactivity.

5. X-ray Adsorption Near Edge Structure

To support oxidation states of Ti and Fe in the discussion above, XANES was used to provide the information. The different XANES spectra present the different electronic states of the chemical bonds in each compound. Fig. 5(a) shows the XANES spectra of Ti standard compounds. The spectrum of standard Ti foil shows a sharp peak at 4,967 eV while standard TiO_2 displays clearly three pre-edge peaks, which corresponds to 1s to 3d transition. The XANES spectrum of Fe doped TiO_2 displayed the characteristic of TiO_2. The

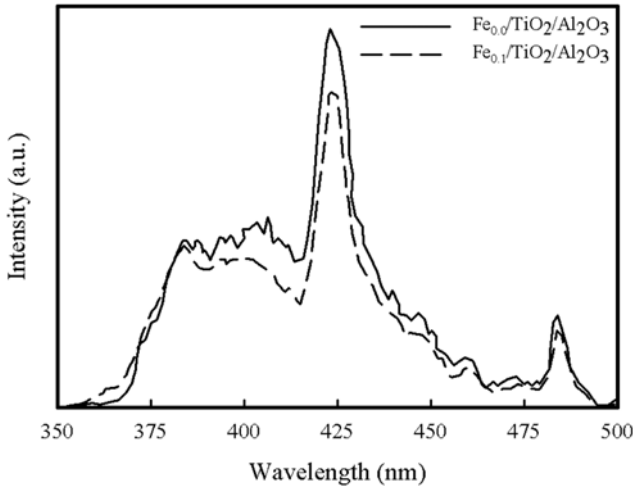

Fig. 4. PL spectra of $Fe_x/TiO_2/Al_2O_3$ beads calcined at 400 °C; Excitation source was at 315 nm He-Cd laser.

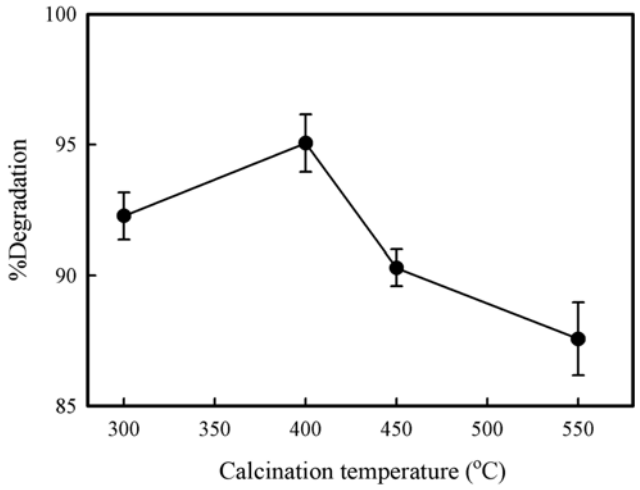

Fig. 6. Degradation of MB for the catalyst $Fe_{0.1}/TiO_2/Al_2O_3$ beads calcined at different temperatures.

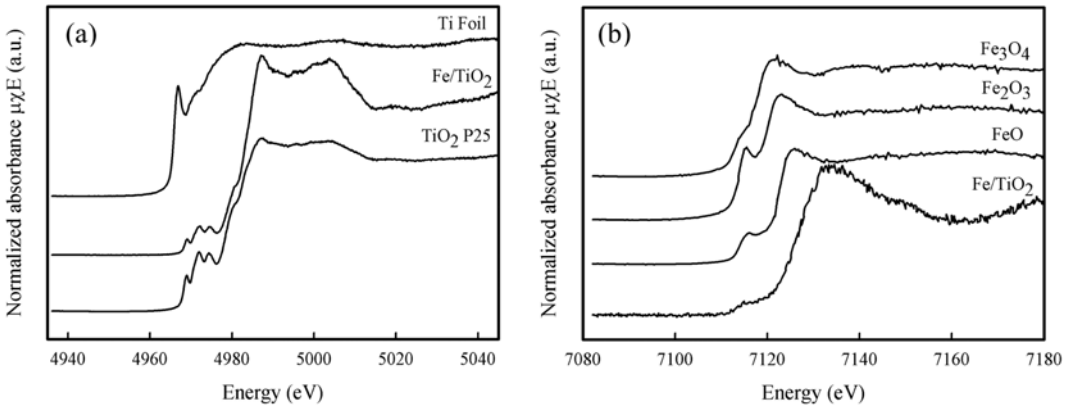

Fig. 5. XANES spectra of Ti K-edge (a) and Fe K-edge (b) compared with standard compounds. Sample: $Fe_{0.1}/TiO_2/Al_2O_3$ beads.

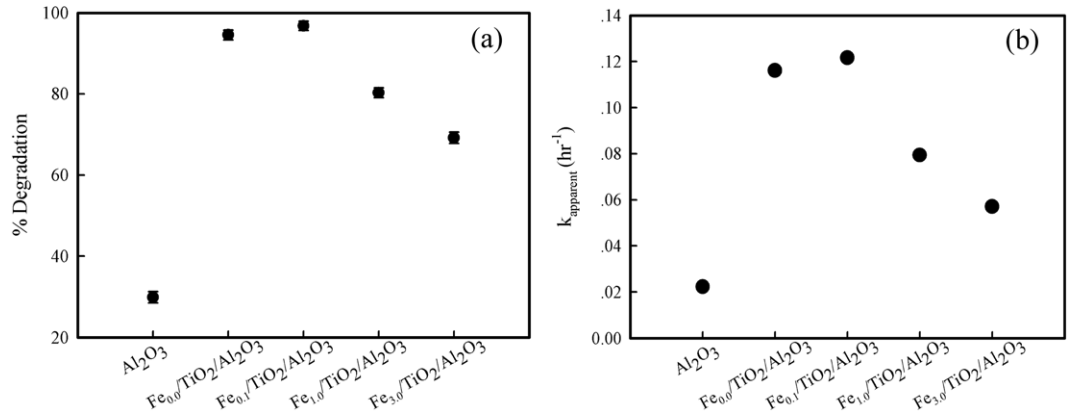

Fig. 7. Performance of $Fe_x/TiO_2/Al_2O_3$ beads in term of (a) %Degradation, (b) apparent kinetic constant.

threshold energy of the sample was the same as in the crystalline TiO_2, indicating that most of the Ti ion were Ti^{4+}. Fig. 5(b) shows the normalized XANES at Fe *K*-edge of Fe compounds. The comparison of sample with standard compounds of FeO, Fe_3O_4, and Fe_2O_3 was carried out. The XANES spectrum of Fe doped TiO_2 photocatalyst shows a weak pre-edge peak at 7,117 eV between FeO and Fe_2O_3, which corresponds to Fe_3O_4 compound. Although this peak was at the same position to that of the bulk Fe_3O_4, the intensity was different due to trace amount of metal doping. This indicated that Fe species were displayed a mixed valence of Fe^{2+} and Fe^{3+} species, as confirmed by the visible white line peak at 7,130 eV, which was the contribution of 1s to 4p transition and referred to the mixed-valence species of Fe^{2+} and Fe^{3+} [16].

6. Photodecomposition of Methylene Blue (MB)

The photodecomposition of MB using a catalyst calcined at different temperatures and different Fe^{3+} loadings was examined. The catalyst calcined at 400 °C gave the highest DE% as presented in Fig. 6. This can be attributed to just the right amount of anatase and rutile present in the catalyst. An optimal blend of these phases then leads to synergy and improved performance. This was due to the enhancement of electron-hole lifetime and the decrease of electron-hole pair recombination.

Fig. 7 shows the effect of Fe^{3+} concentration on the photocatalytic activity of the synthesized catalyst in terms of the k_{app} (from the pseudo-first order kinetics) and DE%. $Fe_{0.1}/TiO_2/Al_2O_3$ gave the highest DE%. Although, the increase in DE% was not very significant to that of $Fe_{0.0}/TiO_2/Al_2O_3$, this result was consistent with the results of the UVDR spectra and PL spectra, which both showed little change in the intensities of the two samples.

On the other hand, the addition of more Fe^{3+} in the TiO_2 proved lethal to the photocatalytic activity of the catalyst. Beyond the optimal dose (0.1% Fe^{3+}), the Fe^{3+} might have increased recombination sites and had an adverse effect on the activity of the catalyst.

CONCLUSION

In summary, Fe^{3+} doped TiO_2 can be efficiently loaded to alumina beads via mechanical coating technique and calcination in air. The catalyst beads have a finer surface compared to alumina. The microstructure of the synthesized catalyst is a combination of rutile and anatase. The optimum calcination temperature is 400 °C and the optimum doping concentration is 0.1 at % Fe^{3+}. The catalyst produced is useful for treating waste water without the need of the post filtration process.

ACKNOWLEDGEMENT

The authors acknowledge the Office of the Higher Education Commission (Targeted Research Initiatives), Thailand, for the financial support.

REFERENCES

1. Y. Long, Y. Lu, Y. Huang, Y. Peng, Y. Lu, S.-Z. Kang and J. Mu, *J. Phys. Chem. C.*, **113**, 13899 (2009).
2. W. S. Nam and G. Y. Han, *Korean J. Chem. Eng.*, **20**, 180 (2003).
3. S. Artkla, K. Wantala, B. Srinameb, N. Grisdanurak, W. Klysubun and J. Wittayakun, *Korean J. Chem. Eng.*, **26**, 1556 (2009).
4. M. Zhou, J. Yu and B. Cheng, *J. Hazard. Mater.*, **137**, 1838 (2006).
5. S. Yin, M. Komatsu, Q. Zhang, F. Saito and T. Sato, *J. Mater. Sci.*, **42**, 2399 (2007).
6. W. Choi, A. Termin and M. Hoffmann, *J. Phys. Chem.*, **98**, 13669 (1994).
7. J.-W. Shi, J.-T. Zheng, Y. Hu and Y.-C. Zhao, *Mater. Chem. Phys.*, **106**, 247 (2007).
8. H. Yoshida, Y. Lu, H. Nakayama and M. Hirohashi, *J. Alloy. Compd.*, **475**, 383 (2009).
9. M. I. Litter and J. A. Navío, *J. Photochem. Photobio. A.*, **98**, 171 (1996).
10. F. R. Feret, D. Roy and C. Boulanger, *Spectro. Acta. B.*, **55**, 1051 (2000).
11. Z. Li, W. Shen, W. He and X. Zu, *J. Hazard. Mater.*, **155**, 590 (2008).
12. M. Zhou, J. Yu and B. Cheng, *J. Hazard. Mater.*, **137**, 1838 (2006).
13. P. Bouras, E. Stathatos and P. Lianos, *Appl. Catal. B-Environ.*, **73**, 51 (2007).
14. B. Liu, L. Wen and X. Zhao, *Mater. Chem. Phys.*, **106**, 350 (2007).
15. T. L. Thompson and J. T. Yates, *Top. Catal.*, **35**, 197 (2005).
16. T.-F. Hsu, T.-L. Hsiung, J. Wang, C.-H. Huang and H. P. Wang, *Nucl. Instrum. Methods Phys. Res. A.*, **619**, 98 (2010).